Increase of reduced nicotinamide adenine dinucleotide fluorescence lifetime precedes mitochondrial dysfunction in staurosporine-induced apoptosis of HeLa cells

Jia-Sin Yu
Han-Wen Guo
Chih-Hao Wang
Yau-Huei Wei
Hsing-Wen Wang

Increase of reduced nicotinamide adenine dinucleotide fluorescence lifetime precedes mitochondrial dysfunction in staurosporine-induced apoptosis of HeLa cells

Jia-Sin Yu,[a] Han-Wen Guo,[a] Chih-Hao Wang,[b] Yau-Huei Wei,[b,c] and Hsing-Wen Wang[a]
[a]National Yang-Ming University, Institute of Biophotonics, Taipei 112, Taiwan
[b]National Yang-Ming University, Institute of Biochemistry and Molecular Biology, Taipei 112, Taiwan
[c]Mackay Medical College, Department of Medicine, SanJhih, Taipei County 252, Taiwan

Abstract. *In vivo* noninvasive detection of apoptosis represents a new tool that may yield a more definite diagnosis, a more accurate prognosis, and help improve therapies for human diseases. The intrinsic fluorescence of reduced nicotinamide adenine dinucleotide (NADH) may be a potential optical biomarker for the apoptosis detection because NADH is involved in the respiration for the mitochondrial membrane potential ($\Delta\Psi$) formation and adenosine-5′-triphosphate (ATP) synthesis, and the depletion of $\Delta\Psi$ and ATP level is the hallmark of apoptosis. We have previously observed the NADH fluorescence lifetime change is associated with staurosporine (STS)-induced mitochondria-mediated apoptosis. However, its relationship with mitochondrial functions such as $\Delta\Psi$, ATP, and oxygen consumption rate is not clear. In this study, we investigated this relationship. Our results indicate that the NADH fluorescence lifetime increased when $\Delta\Psi$ and ATP levels were equal to or higher than their values of controls and decreased before the depletion of $\Delta\Psi$ and ATP, and the oxygen consumption rate did not change. These findings suggest that the increased NADH fluorescence lifetime in STS-induced cell death occurred before the depletion of $\Delta\Psi$ and ATP and activation of caspase 3, and was not simply caused by cellular metabolic change. Furthermore, the NADH fluorescence lifetime change is associated with the pace of apoptosis. © *2011 Society of Photo-Optical Instrumentation Engineers (SPIE).* [DOI: 10.1117/1.3560513]

Keywords: ATP; apoptosis; mitochondrial dysfunction; NADH fluorescence lifetime; mitochondrial membrane potential; oxygen consumption.

Paper 10494RR received Sep. 9, 2010; revised manuscript received Jan. 29, 2011; accepted for publication Feb. 3, 2011; published online Mar. 29, 2011.

1 Introduction

Apoptosis is a highly regulated multistep biological process and energy-dependent form of cell death.[1] Dysregulation of apoptosis causes human diseases including autoimmunity, neurodegeneration, and heart disease when cells abnormally die.[2] When tissue cells are resistant to apoptosis, it may promote cancer growth and impede the effectiveness of cancer therapies.[2] In a broad view, apoptosis can operate via two pathways, one is mitochondria-mediated and the other is receptor-mediated but mitochondria-independent.[3] In the mitochondria-dependent pathway, an external insult acts on the mitochondrion, with or without the action of proapoptotic proteins such as Bak and Bax, to cause cytochrome *c* release from the mitochondria to the cytoplasm, which is accompanied by the loss of the mitochondrial membrane potential. Released cytochrome *c* interacts with apoptotic protease-activating factor 1, ATP, and pro-caspase 9 to form the apoptosome. This apoptosome then activates a cascade of cellular destruction events, beginning with the activation of death-execution effector caspases, such as caspase 3, followed by the activation of downstream caspases, ultimately resulting in the hallmark of apoptosis including condensation of nuclear and cytoplasmic contents, fragmentation of nuclear DNA, and membrane blebbing.[3,4]

Insight into the molecular mechanism of apoptosis has opened new avenues to develop diagnostic, prognostic, and therapeutic tools for management of human diseases.[1,5,6] For example, apoptosis-based therapies have been used in the treatment of degenerative, neoplastic, and autoimmune disorders.[2,7] To keep track of the outcome of apoptosis-based therapy, a biopsy specimen combined with *in vitro* assays is often used to detect apoptotic signals in certain molecular pathways preceding morphological changes. For the detection of apoptosis *in vivo*, molecular imaging techniques were used to image caspase activity or phosphatidylserine (PS) exposure.[4,8] Imaging the activation of the caspase cascade such as caspase 3 activity has been demonstrated in animals using positron emission tomography (PET).[9,10] However, no human data have ever been published and caspase 3 activation is not necessarily unique to apoptosis.[11,12] On the other hand, the PS externalization is thought to be an early event in apoptosis that closely follows caspase 3 activation.[4] Annexin V has been the most widely used PS-targeting human protein and allows MRI-, optical-, radionuclide-, and PET-detection via superparamagnetic iron oxide nanoparticle-, fluorescence-, radio-, and (^{18}F)-labeled techniques, respectively. It has been used in phase I and phase

Address all correspondence to: Hsing-Wen Wang, National Yang-Ming University, Institute of Biophotonics, 155 Li-Nong St., Sec. 2, Taipei 112 Taiwan. Tel.: 886-2-2826-7378; Fax: 886-2- 2823-5460; E-mail: hwwang2@ym.edu.tw.

II clinical trials as a potential early surrogate marker of therapeutic efficacy in nonsmall cell lung cancer and non-Hodgkin's lymphoma.[13]

We have investigated the potential of using reduced nicotinamide adenine dinucleotide (NADH) fluorescence lifetime as a new *in vivo* biomarker to detect apoptosis at the early phase. NADH is involved in the respiration in mitochondria to generate membrane potential and synthesize ATP. Depletion of $\Delta\Psi$ and ATP are key features of the execution of apoptosis. NADH fluorescence lifetime (τ) is attributed to two major lifetime components: free NADH exhibiting a shorter lifetime, τ_1 ~0.4 to 0.5 ns, and bound NADH exhibiting a longer lifetime, τ_2 ~2 to 8 ns. These lifetime components have been associated with the metabolic activities and neoplasm.[14,15]

In one of our previous studies, staurosporine (STS)-induced apoptosis in HeLa cells was used as the model of the mitochondria-mediated apoptotic pathway that involves cytochrome *c* release, $\Delta\Psi$ decrease, caspase 3 activation, and nuclear DNA fragmentation.[16] We observed an immediate increase of NADH fluorescence lifetime within the first 15 min after 1 μM STS induction and then a decrease at our 2nd acquired time point (i.e., 15 to 30 min), which occurred earlier than caspase 3 activation and expression of annexin V.[17] The mechanism behind this NADH fluorescence lifetime change is unknown and still awaits clarification. In this study, we investigated the time course relationship of NADH fluorescence lifetime and mitochondrial functions including $\Delta\Psi$, ATP content, and oxygen consumption rate of mitochondria after STS-induced apoptosis. Mitochondrial dysfunction (e.g., $\Delta\Psi$ decline) is essential to kill cells by STS regardless of the inhibition of caspase.[18] Furthermore, the extent of changes in $\Delta\Psi$ and ATP in mitochondria determined the pathway of the cell death, i.e., apoptosis versus necrosis.[19] Thus, exploring the time course of these signals related to the mitochondrial function may help understand the origin of NADH fluorescence lifetime change in the mitochondria-mediated apoptosis.

2 Materials and methods

2.1 Cell Cultures and Experiments

Cell preparation and NADH fluorescence lifetime imaging microscopy (FLIM) were conducted as previously reported.[17] Human HeLa cells were cultured in Dulbecco's modified Eagle's medium (DMEM; Gibco, Invitrogen Corp., Carlsbad, California) containing 100 units/ml penicillin G, 100 μg/ml streptomycin sulfate, 0.5 μg/ml amphotericin B, and 5% fetal bovine serum (FBS) (Biological Industries, Kibbutz Beit Haemek, Israel) at 37 °C in a humidified atmosphere with 5% CO$_2$. At 24 h before NADH fluorescence lifetime imaging and drug treatments, cells at a density of 2×10^4 cells/cm^2 were seeded onto 24-mm diameter round glass cover slips (Paul Marienfeld GmbH & Co., Lauda-Konigshofen, Germany), which had been coated with 200 μl undiluted FBS per cover slip. These cover slips were then kept in dishes and cultured in DMEM inside an incubator for 24 h until cells were completely attached onto the cover slip and in the early log phase of cell proliferation. Immediately before taking NADH fluorescence images, cells were washed twice using a phosphate-buffered saline (PBS) solution and then transferred to a cell chamber designed for viewing live cells. An aliquot of 1 ml of 5 mM

4-(2-hydroxyethyl)-1-piperazineethanesulfonic acid (HEPES) buffer (5 mM KCl, 140 mM NaCl, 2 mM CaCl$_2$, 1 mM MgCl$_2$, 10 mM glucose, *p*H 7.4) was used to nourish cells without light absorption of the red color of the culture medium during fluorescence lifetime imaging. Additional measurements were performed using PBS in the same field of view (FOV) of control cells to ensure HEPES does not affect the lifetime measurement (data not shown). All of the images were acquired at room temperature to optimize the NADH fluorescence intensity.[20] The temperature effect has been carefully considered in our previous study that the results of NADH fluorescence lifetime before and within the first 15 min after STS treatment were not affected by the room temperature condition (Ref. 17, Tables 1 and 2). We also observed no temperature effect on the NADH fluorescence lifetime of control and 1 μM STS-treated cells at later time points up to 2 h (data not shown). The physiological temperature was maintained with the hot air blown into the plexiglass microscope stage incubator, whereas both the stage and the lens were heated simultaneously. Even distribution of the hot air inside the incubator was ensured by a couple of small fans attached to the box walls. The temperature was read by a thermal coupler from a reference well, filled with distilled water, and the air blow volume was adjusted correspondingly by the control unit.

Our previous study of HeLa cells treated with 1 μM STS (Sigma-Aldrich, St. Louis, Missouri) showed an immediate NADH fluorescence lifetime increase (i.e., within the first 15 min) during a continuous 2 h FLIM imaging period at room temperature. We would like to study this lifetime change at a slower pace and hypothesized that the pace of this lifetime change depends on the STS concentration. We tested STS doses at 1, 25, 50, and 100 nM. We found that the NADH fluorescence lifetime immediately increased at the concentration of 100 nM. At 50 nM of STS a gradually increased NADH lifetime was observed within 2 h. At 1 and 25 nM STS dose levels, the NADH fluorescence lifetime did not change much within a 2 h time frame. Thus we chose 50 nM as the "lower" dose for this study to compare with previously used 1 μM as the "higher" dose. Time-lapsed NADH fluorescence lifetime images were obtained at the same site (same FOV) before, immediately after (0 to 15 min), and up to 2 h after treatment of HeLa cells with STS. The FOV of each image was 100$\times$100 μm (256$\times$256 pixels). Control images of cells were taken before STS treatment. The acquisition time of each image was 600 s to ensure acquiring enough photons for reliable NADH fluorescence lifetime analysis.

2.2 Mitochondrial Dysfunction, Cell Preparation, and Polymerase Chain Reaction Analysis

Human cytoplasmic hybrids (cybrids) harboring two different proportions (0 versus ~56%) of 4,977 base pair-deleted mitochondrial DNA (mtDNA) were previously made by fusing mtDNA-less human osteosarcoma cells with enucleated skin fibroblasts that has been established from a patient with clinically proven chronic progressive external ophthalmoplegia syndrome.[21] The exact proportion of 4,977 bp-deleted mtDNA in each of the cybrids used for this study was confirmed by polymerase chain reaction (PCR) analysis or by Southern hybridization according to previous reports.[21,22] The cybrids were grown in DMEM supplemented with 5% FBS, 100 μg/ml pyruvate, and 50 μg/ml uridine and incubated at 37 °C in a humidified atmosphere with 5% CO$_2$.

2.3 Caspase 3 Activity Assay

Cells were disintegrated in 100 μl lysis buffer (12.5 mM Tris-HCl, 1 mM dithiothreitol, 0.125 mM ethylenediaminetetraacetic acid (EDTA), 5% glycerol, and an aliquot of complete protease inhibitor mixture, (Roche Applied Sciences, Mannheim, Germany), pH 7.0) on ice for 30 min and centrifuged at 9000 g for 10 min at 4 °C. An aliquot of 50 μg protein was incubated with 20 μM Ac-DEVD-AFC (Calbiochem, San Diego, California), a fluorescent substrate of caspase 3, in 500 μl of assay buffer (50 mM Tris-HCl, 1 mM EDTA, and 10 mM EGTA, pH 7.0) at 37 °C for 30 min in the dark. The fluorescence intensity of the product was determined by the spectrofluorometry (Hitachi F-3000, Tokyo, Japan) at an excitation wavelength of 380 nm and an emission wavelength of 508 nm as described previously.[21]

2.4 Measurements of intracellular ATP content

The intracellular ATP content was measured by means of cytosol- and mitochondria-targeted luciferase using a bioluminescent somatic cell ATP assay kit (Sigma-Aldrich, St. Louis, Missouri). Intracellular ATP was released by mixing an aliquot of 50 μl of viable cell suspension collected at different time points before and after STS treatment with 150 μl of somatic cell releasing buffer. Half of the mixture was then transferred into a black 96-well plate (OptiPlate-96F, Packed Biosciences, Perkin-Elmer, Foster City, California) containing 100 μl of ATP assay mix per well. The chemiluminescence intensity was measured by the Victor^2 1420 multilabel counter (Perkin Elmer Life and Analytical Sciences, Waltham, Massachusetts). The luminescence intensity was normalized to the total number of cells.

2.5 Measurements of Mitochondrial Membrane Potential ($\Delta\Psi$)

The membrane potential of mitochondria ($\Delta\Psi$) was determined by the use of 5,5′,6,6′-tetrachloro-1,1′3,3′-tetraethylbenzimidazolyl carbocyanine iodide (JC-1; Molecular Probes, Eugene, Oregon). The cell pellet was dispersed into fresh DMEM containing 2 μM JC-1 for 30 min at 37 °C. Cells were then washed twice with PBS, re-suspended in 200 μl PBS and transferred into a black OptiPlate-96F 96-well plate (Packed Bioscience, Perkin-Elmer) to measure $\Delta\Psi$ by the Victor^2 1420 multilabel counter (PerkinElmer Life and Analytical Science, Waltham, Massachusetts). J-monomer fluorescence was excited and emitted at 485 nm and 535 nm, respectively. J-aggregate fluorescence was excited and emitted at 544 nm and 590 nm, respectively. The $\Delta\Psi$ was determined by the ratio of the fluorescence intensity between the J-aggregate and the J-monomer.

2.6 Measurements of the Oxygen Consumption Rate

The oxygen consumption rate was measured by using the 782 oxygen meter (Strathkelvin Instrument, Motherwell, UK). An aliquot of 4×10^5 cells was re-suspended in 330 μl of assay buffer (125 mM sucrose, 65 mM KCl, 2 mM MgCl$_2$, 20 mM phosphate buffer, pH 7.2) and the cell suspension was then transferred into the incubation chamber. An aliquot of 0.0006% digitonin (Sigma-Aldrich, St. Louis, Missouri) was added to permeabilize the plasma membrane of the cells. The rate of substrate-supported oxygen consumption was measured after injecting 17 mM glutamate and 17 mM malate into the chamber

as the electron donors. The state 3 respiration rate (i.e., the state of ATP synthesis) was then established and measured after injection of an additional 1 mM ADP.[23]

2.7 NADH Fluorescence Lifetime Imaging Microscopy and Data Analysis

Time-domain FLIM was performed using a 60×1.45NA planapochromat oil objective lens (Olympus Corp., Tokyo, Japan) on a modified 2-photon laser scanning microscope (FV300 with the IX71 inverted microscope, Olympus Corp., Japan) as described previously.[17] In this study, samples were excited at 740 nm (2-photon) by a mode-locked Ti:Sapphire Mira F-900 laser, pumped by a solid-state continuous wave 532 nm Verdi laser (both from Coherent Inc., Santa Clara, California). The scanning speed of the FV300 was controlled externally by a function generator (AFG310, Tektronix Inc., Beaverton, Oregon).

NADH fluorescence photons were detected using a bandpass filter of 447 $\pm$ 30 nm (Semrock Inc., Rochester, NewYork) in a non-descanned mode by a photon counting photomultiplier (H7422P-40, Hamamatsu Photonics K.K., Hamamatsu, Japan). Time-resolved detection was conducted by the single-photon-counting SPC-830 PC board (Becker & Hickl GmbH, Berlin, Germany). Additional short pass and infrared cut-off filters were used to reject reflected or scattered excitation light at 740 nm. The average laser power of ∼3 to 5 mW was used at the focal plane of the objective, which is lower than the reported laser power of two-photon damage[17] and was found optimal for the prevention of photobleaching.

NADH lifetime data were analyzed with the commercially available SPCImage v2.8 software package (Becker & Hickl GmbH, Berlin, Germany) that convoluted a double-exponential model function, $F(t) = a_1 e^{-t/\tau_1} + a_2 e^{-t/\tau_2}$, and the instrument response function, I_{instr}, and then fitted the convoluted results to the experiment data to extract lifetime parameters τ_1, τ_2, a_1, and a_2. Here $a_1 e^{-t/\tau_1}$ and $a_2 e^{-t/\tau_2}$ represent the contributed fluorescence decays from free and bound NADH, respectively, τ_1 and τ_2 represent their corresponding lifetimes, and a_1 and a_2 are the corresponding relative amplitudes. I_{instr} was measured using a second-harmonic generated signal from a periodically poled lithium niobate crystal as previously reported.[24] A representative fluorescence decay curve, the fit, and the residual are shown in Fig. 1(c) of our previous study[17] to show the quality of the lifetime fit. A three or higher component exponential model function was tested to see if it provided a better fit in the lifetime micrograph of control cells. However, the lifetime parameters τ_1, τ_2, a_1, and a_2 remained almost the same as those from the two-component fit. The 3rd or higher corresponding relative amplitudes showed a relatively small number.

3 Results

3.1 Cell Morphological Change and Caspase 3 Activation Confirmed STS-Induced Apoptosis

We confirmed 1 μM STS-induced apoptosis in our previous study by cell morphological change and caspase 3 activation.[17] To confirm that the cell death pathway is through apoptosis at 20 times lower STS dose (i.e., 50 nM) in this study, we examined the cell morphology and measured caspase 3 activity as
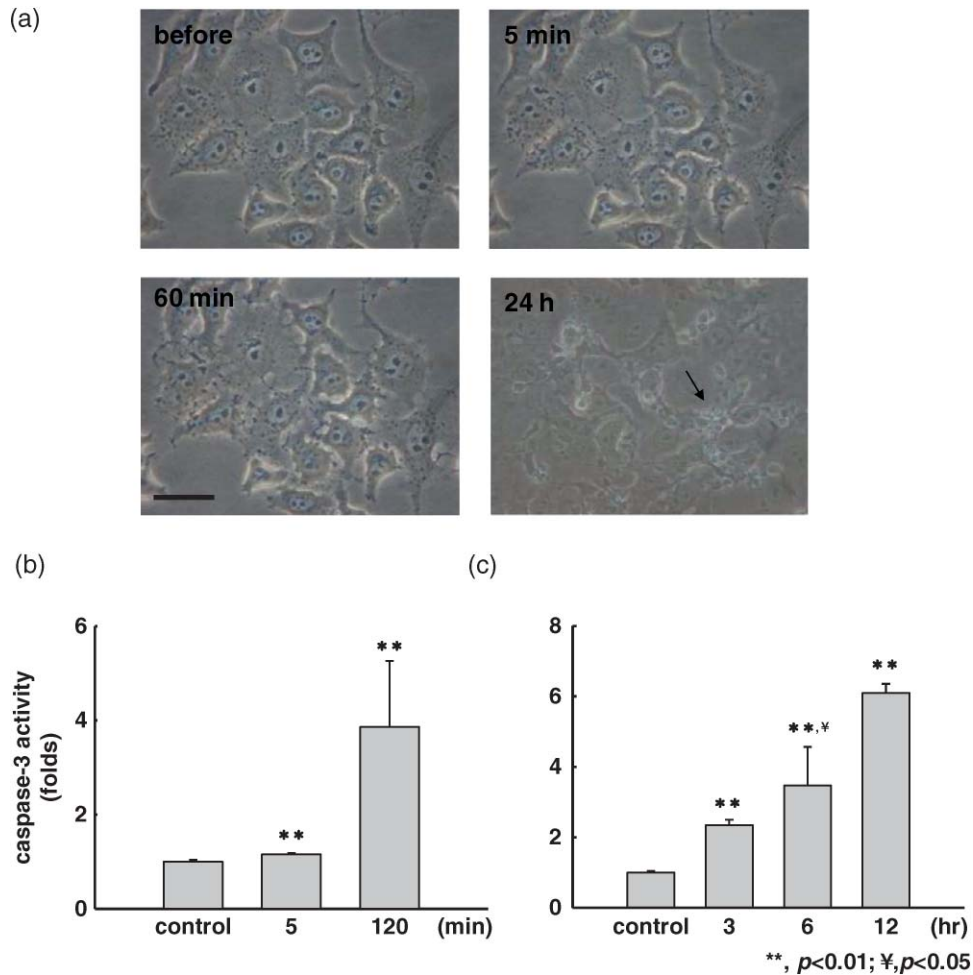
Fig. 1 (a) The morphology of HeLa cells after treatment with 50 nM STS. The scale bar in (a) is 30 μm. Arrow indicates cell blebbing during apoptosis. Normalized caspase 3 activity of HeLa cells after treatment of cells with 1 μM (b) and 50 nM (c) STS, respectively. Symbols ** and ¥ indicate a significant p-value by comparing to the control and the previous time point, respectively.

described previously. Figure 1(a) depicts the light microscopic images of HeLa cells before and 5 min, 60 min, and 24 h after 50 nM STS treatment. All images were taken at the same magnification. The typical hallmarks of apoptotic cells, cell shrinkage and blebbing [arrow in Fig. 1(a)], were observed at a 24 h time point. Fig. 1(c) shows the normalized caspase 3 activities of HeLa cells before (controls) and after STS treatment at 50 nM, as well as at 1 μM [Fig. 1(b)] for comparison. As expected, caspase 3 was activated slower when cells had been exposed at a lower STS dose, in which it required up to 6 h to become 3 folds or higher than controls after 50 nM STS treatment rather than 2 h at 1 μM. We added an additional measurement at 5 min after 1 μM STS treatment and observed a significant higher caspase 3 activity at 1.16 ± 0.02 folds than controls (p value $= 5.62 \times 10^{-4}$), which indicates an immediate apoptotic process started at 1 μM STS treatment.

3.2 NADH Fluorescence Lifetime Increased in STS-induced Apoptosis in a Dose-Dependent Manner

Figure 2 shows the representative time course images of NADH fluorescence lifetime at the same field of view (FOV)

[Fig. 2(A)] and the corresponding normalized lifetime histograms [Fig. 2(B)] before and after treatment with 50 nM STS. The histograms with label (a) to (f) correspond to the time course lifetime images (a) to (f) in Fig. 2(A), respectively. The fluorescence signals in the cytoplasm display punctuate perinuclear patterns, which were attributed to mitochondria-associated NADH.[14,25] No fluorescence is seen in the nuclei or on the nuclear membrane. Each pixel represents the mean lifetime (τ_m) of the short (τ_1) and long (τ_2) lifetime components weighted by their relative contributions a_1 and a_2, respectively, such that $\tau_m = (a_1\tau_1 + a_2\tau_2)/(a_1 + a_2)$. The scale of the color mapping was chosen such that the blue color represented the longer lifetime (maximum 4000 ps) and the red color presented the shorter lifetime (minimum 200 ps). The "dark pixels" are due to no lifetime information there and thus no colors were assigned. No lifetime information can be due to a lack of NADH fluorescence signal from the pixels such as those in the medium and nuclear areas, and/or not enough NADH fluorescence intensity (or photon counts) for a reliable lifetime calculation. The color-coded lifetime images exhibit a gradual blue shift (increased lifetime) from the image taken at the time of controls to that taken at 115 to 125 min after 50 nM STS treatment. The normalized histograms of the mean lifetime
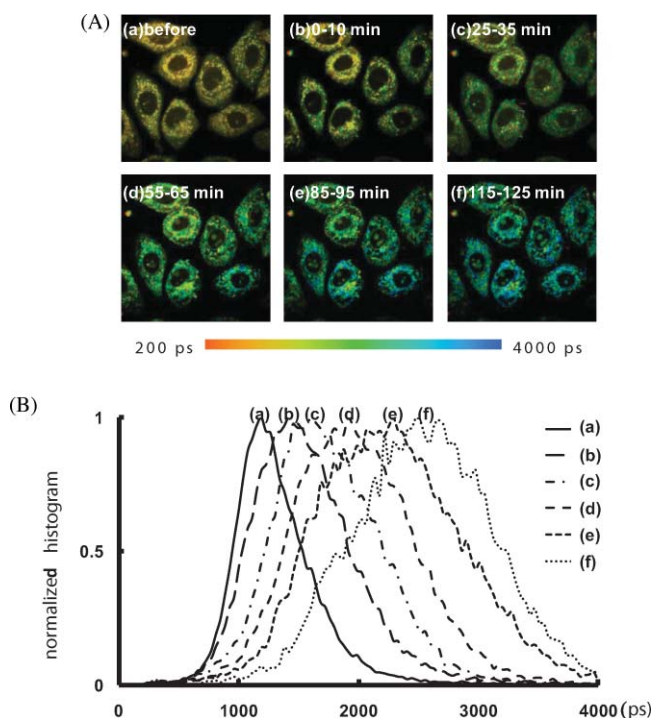
Fig. 2 Effect of STS treatment on the NADH fluorescence lifetime of HeLa cells. (A) Two-photon FLIM micrographs of HeLa cells from the same sites before (a), and 0 to 10 min (b), 25 to 35 min (c), 55 to 65 min (d), 85 to 95 min (e), and 115 to 125 min (f) after treatment with 50 nM STS. The field of view of each image is 100×100 μm. (B) The normalized histograms of τ_m over the 256×256 pixel lifetime image were plotted from curves a to f corresponding to each image at all time points shown in (A).

(τ_m) from all pixels of the same FOV images taken at different time points show a peak (τ_{peak}) shift from ~1100 to ~2700 ps [Fig. 2(B)]. The full-width-at-half-maximum (FWHM) was ~500 ps at the time of controls but become broader to be ~1400 ps at 115 to 125 min after the STS treatment indicating that the inhomogeneous lifetime distribution within cells varied with time.

Similar results were repeatedly observed in a total of eight samples at each time point and summarized in Fig. 3(a), which plot the mean and standard deviation (STD) of the median lifetime values from the normalized τ_m histograms. The time labeled at the x-axis was assigned as the mean value over the image acquisition time (i.e., 10 min). For example, 5 min represents the data point acquired at 0 to 10 min after treatment. Additionally, NADH mean fluorescence lifetimes at 3 and 4 h post-STS induction are shown in the same figure averaging over a total of three samples at each of these two time points. These data were taken from cells that had been subject to STS treatment and incubated in the incubator before FLIM. Thus they did not have the same FOV as other time points for each sample. However, because we compared the average result of at least 20 cells and the standard deviations at these later time points are similar to those at controls, these data well represented the trend of the NADH lifetime change at these later time points. Overall, Fig. 3(a) shows that NADH fluorescence lifetime increased for up to 2 h and then a decreased at 3 and 4 h post-exposing at 50 nM STS. The mean τ_m values up to 2 h after 50 nM STS treatment

are significantly different from those values of controls (p value $<1.0 \times 10^{-9}$). We repeated our previous study using 1 μM STS and the mean τ_m ($\pm$ STD) values were plotted in the same figure for comparison. Consistent with our previously published data, an immediate increase in the lifetime within 10 min followed by a decrease was observed. Although the trend of an increase and then a decrease in the lifetime was similar at both 50 nM and 1 μM STS treatment, the amplitude of the increase in NADH fluorescence lifetime was dose-dependent. The mean τ_m at 1 μM STS dose increased to 3287 ± 296 ps but the mean τ_m at 50 nM STS only increased to 2182 ± 284 ps. In addition, the time to reach the maximal τ_m at 1 μM STS dose was shorter than that at 50 nM (5 min versus 2 h), as well as that τ_m decreased earlier at a higher STS dose. The results in Figs. 1 and 3 imply that the NADH fluorescence lifetime change followed the kinetics of the apoptosis. The higher the STS dose used, the earlier the apoptotic process started, and the earlier the caspase 3 was activated.

3.3 NADH Fluorescence Lifetime Increase was Attributed to Decreased Free-to-Bound NADH Ratio and Increased Fluorescence Lifetime of the Protein-Bound NADH

To understand the mechanism behind the increase of NADH fluorescence lifetime after STS treatment, we analyzed the lifetime component distribution further by examining the histogram of a_1-to-a_2 ratio, τ_1, and τ_2 that represented free-to-bound NADH ratio, free NADH lifetime, and bound NADH lifetime, respectively. Similar to obtaining the mean τ_m at each time point in Fig. 3(a), we first obtained the median value from the a_1-to-a_2 ratio, τ_1, and τ_2 histograms of each fluorescence lifetime image, and then we calculated the mean value and standard deviation over three to eight samples at each time point. The results were plotted in Figs. 3(b)–3(d), which show a significant decrease in the a_1-to-a_2 ratio and increase in τ_1 and τ_2 within 2 h of 50 nM STS treatment. At 3 to 4 h, these lifetime components (a_1-to-a_2 ratio, τ_1, and τ_2) returned to values similar to those of controls. This indicates that more bound NADH than free NADH were created during the first 2 h of 50 nM STS-induced apoptosis and the lifetime of bound NADH became longer as well. Vishwasrao et al.[26] reported three types of enzyme-bound NADHs using 4-component lifetime analyses in hippocampal slices where bound NADH has a lifetime greater than 1000 ps. The increase of τ_1 to be greater than 750 ps at 2 h post treatment in Fig. 3(c) may imply the tendency of free NADH becoming bound form (i.e., the long lifetime component). Similar plots for cells treated with 1 μM STS were shown in the same figure for comparison and they show similar trends as those with 50 nM STS. Overall, the data suggest that the increase in NADH fluorescence lifetime observed in STS-induced apoptosis is due to both an increased amount of bound NADH components and a redistribution of protein-bound NADH molecules to different enzyme binding sites. Furthermore, Fig. 3 indicates that these changes (i.e., increased τ_m, τ_1, τ_2 and decreased a_1-to-a_2 ratio) occurred quickly after STS was introduced because the steepest slopes appeared in the early time point, in which the x-axis of the figure is plotted to be proportional to the time scale.
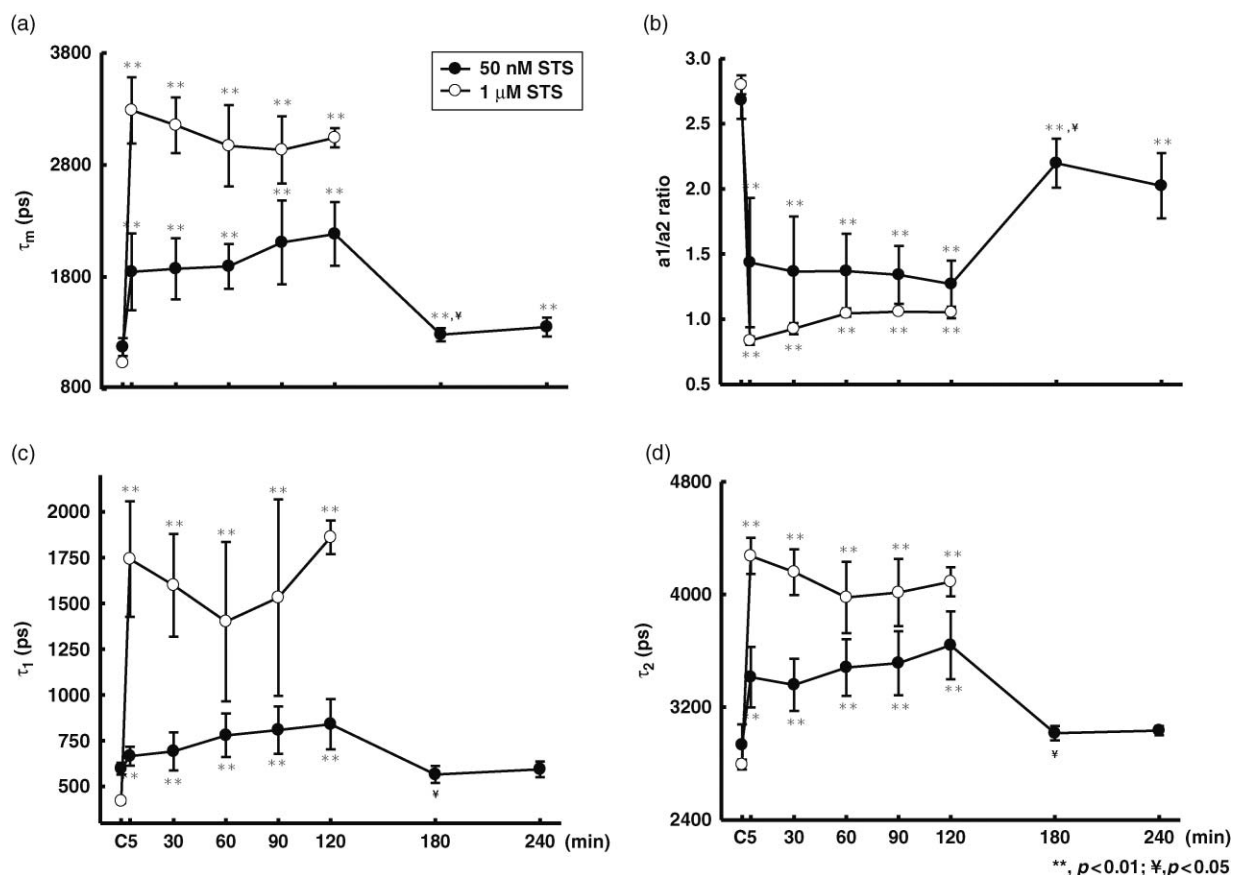
Fig. 3 The plots of the mean and standard deviation of the τ_m (a), a_1-to-a_2 ratio (b), τ_1 (c), and τ_2 (d) over 3 to 12 fields of view as the function of time in 50 nM STS-treated cells. The time axis was plotted proportional to the linear time scale. The τ_m, a_1-to-a_2 ratio, τ_1, and τ_2 of NADH fluorescence of HeLa cells treated with 1 μM STS was plotted in the same figure for comparison. In the x-axis, "C" represents the time point before treatment or the control. Symbols ** and ¥ indicate a significant p-value by comparing to the control and the previous time point, respectively.

3.4 NADH Fluorescence Lifetime Increased During STS-Induced Apoptosis in Cells With Mitochondrial Dysfunctions

Figure 4(a) shows the time course mean τ_m of cybrids with mitochondrial dysfunction, 1-3-16 and 51-10, before and after 100 nM STS treatment. 1-3-16 cell is the control cybrid having 0% of 4,977 bp-deleted mtDNA and the 51-10 had 56% of 4977 bp-deleted mtDNA, which was confirmed by PCR analysis shown in Fig. 4(b). In a previous study of apoptosis induced by 100 nM STS,[21] the 51-10 cybrid had an approximately 1.5 times higher caspase 3 activity than did the 1-3-16 cybrid at 6 h after the treatment. Figure 4(a) shows that the τ_m of 51-10 cybrids increased 5 min after the STS induction from 1829 $\pm$ 295 ps at controls to 2377 $\pm$ 296 ps. Consistent with the STS dose-dependent results in Fig. 3(a) where apoptosis occurred earlier and the maximal NADH fluorescence lifetime value was higher at a higher concentration of STS, Fig. 4(b) implied that the more severe the mitochondrial dysfunction was, the earlier the apoptosis started, and the higher the maximal NADH fluorescence lifetime increased. However, unlike the STS dose-dependent results in Fig. 3(a) that the maximal mean τ_m occurred at different time points for different STS doses (5 min at 1 μM STS versus 2 h at 50 nM), the maximal τ_m values in both hybrids occurred at the same time point, i.e., 5 min after the 100 nM STS treatment. This is likely because of the STS dose used. We observed an immediate increase of NADH fluorescence lifetime to maximal values when STS at 100 nM or higher concentration was applied in HeLa cells (data not shown).

3.5 NADH Fluorescence Lifetime Kinetic Change Started Earlier Than $\Delta\Psi$ and ATP Change

Mitochondrial membrane potential ($\Delta\Psi$) disruption and ATP depletion are two key steps toward STS-induced apoptotic pathway before caspase 3 activation.[27–29] In order to study their relationship with the NADH fluorescence lifetime change, we measured the time course of $\Delta\Psi$ and ATP level before and after both 1 μM and 50 nM STS treatments in HeLa cells as shown in Fig. 5. All measurements were shown relative to the control which was normalized to a value of 1.0. In Fig. 5(a) at 1 μM STS treatment, $\Delta\Psi$ dropped approximately 20% in 15 min with statistical significance and dropped more than 50% 18 h later. At the same STS dose, ATP did not show significant depletion until 1.5 h or later that the ATP level was 85 $\pm$ 9% relative to the control at 1.5 h and became 32 $\pm$ 20% at 8 h [Fig. 5(c)]. Compared with the NADH fluorescence lifetime change at the same STS dose [1 μM in Fig. 3(a)], the NADH fluorescence lifetime kinetic change (i.e., immediately increased and then decreased) did not seem to correlate with either $\Delta\Psi$ or ATP changes. But the trend of NADH fluorescence lifetime decrease after 30 min
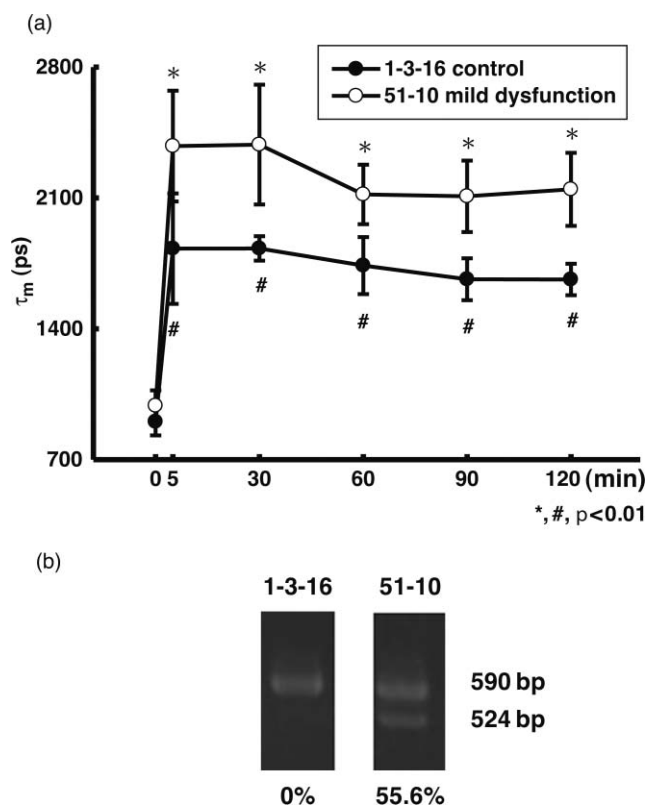
Fig. 4 (a) The plot of the mean and standard deviation of the τ_m over three fields of view as the function of time in 100 nM STS-treated cybrids, 1-3-16 and 51-10, which had 0% and 56%, respectively, of 4977 bp-deleted mtDNA that had been confirmed by PCR analysis (b).

of STS treatment is similar to that of decreased $\Delta\Psi$ at as early as 15 min after the treatment and that of decreased ATP at 1.5 h or later.

Under 50 nM STS treatment, $\Delta\Psi$ significantly increased to $118 \pm 13\%$ and $125 \pm 13\%$ at 2 and 8 h, respectively, and then decreased to $80 \pm 12\%$ at 24 h and to $35 \pm 13\%$ at 72 h after the treatment [Fig. 5(b)]. Different from the $\Delta\Psi$ change, the ATP level tended to increase within the first 2 h, but not statistically significant, and then dropped to ~70% or lower of the control value at 8 h or later after the treatment [Fig. 5(d)]. The trend of the increase and then decrease in NADH fluorescence lifetime at the same STS dose seemed to follow the trend of the increase then decrease of $\Delta\Psi$ and ATP. However, the time to reach the maximal value is shorter for NADH fluorescence lifetime (i.e., ~2 h) than for $\Delta\Psi$ (i.e., ~8 h). For ATP, its level stayed constant or tended to increase while the NADH fluorescence lifetime increased in the first 2 h.

3.6 The Substrate-Supported Oxygen Consumption Rates, State 3 Respiration, and the Mitochondrial Respiration Uncoupling Show No Significant Change After 50 nM STS Treatment

We measured the mitochondrial oxygen consumption rate of 50 nM STS-treated HeLa cells at 8 min, 30 min, 1, 1.5, 2, and 8 h as shown in Table 1. Substrate-supported oxygen consumption rate and State 3 respiration were measured by adding

substrates of glutamate/malate and glutamate/malate plus ADP, respectively. Glutamate/malate provided the electrons to Complex I to increase the rate of oxygen consumption. The addition of ADP was to evaluate the Complex V function that pumps protons from mitochondrial inter-membrane space back to the matrix and thereby generates ATP. Overall speaking, the substrate-supported (i.e., State 2) oxygen consumption rate and State 3 respiration rate fluctuated and did not show a significant increase or decrease within 8 h of treatment with 50 nM STS. As expected, the oxygen consumption rate in the State 3 respiration was higher than that in State 2 when cells were added with substrates only. We divided the State 3 respiration rate by the State 2 respiration rate that reflected how well the coupling was between mitochondrial respiration and ATP synthesis. The coupling of mitochondrial respiration shows no significant difference between controls and STS-treated cells at all time points measured.

4 Discussion

The main goal of the present study was to investigate the relationship between the NADH fluorescence lifetime change and mitochondrial dysfunction in STS-induced apoptosis. We obtained the time course measurement of NADH fluorescence lifetime, mitochondrial membrane potential ($\Delta\Psi$), ATP level, and caspase 3 activity in HeLa cells before and after STS treatment at a higher (1 μM) and lower (50 nM) dose. We also measured the NADH fluorescence lifetime change in cybrids harboring two different portions (0 versus ~56%) of 4977 bp-deleted mtDNA before and after treatment with a fixed dose of STS at 100 nM. The results show that 50 nM STS delayed the increase of NADH fluorescence lifetime and caspase 3 activity and delayed the decrease of $\Delta\Psi$ and ATP level, as compared to cells treated with the higher STS concentration at 1 μM. The slower (or the faster) the STS-induced apoptosis proceeded, the slower (or the faster) the NADH fluorescence lifetime increased, and the lower (or the higher) amount of the maximal lifetime was reached. Cybrids harboring 0% of 4977 bp-deleted mtDNA showed a lower maximal lifetime increase compared to cybrids harboring ~56% of 4,977 bp-deleted mtDNA. In a previous study,[21] cybrids with a higher proportion of 4977 bp-deleted mtDNA showed a higher caspase 3 activity after 6 h of 100 nM STS treatment indicating a faster apoptotic process. Overall, the extent of the increase of NADH fluorescence lifetime due to STS-induced apoptosis is related to a faster apoptosis kinetic due to either the higher concentration of STS or a more pronounced dysfunction of mitochondria in the present study.

However, the time course change of NADH fluorescence lifetime does not seem to associate with that of either ATP or $\Delta\Psi$. While exposing HeLa cells to 1 μM STS, both $\Delta\Psi$ and ATP started decreasing significantly at 15 min and 1.5 h, respectively, after the treatment. At the condition of 50 nM STS where the apoptosis occurred slower so that we could better compare the time course change of the NADH fluorescence lifetime and mitochondrial functions, the $\Delta\Psi$ showed an increase and then a decrease pattern, but $\Delta\Psi$ did not reach its maximum until 8 h after treatment which was 6 h later than the NADH fluorescence lifetime reached its plateau. The ATP content tended to increase at 2 h after the 50 nM STS treatment but this increase was not statistically significant. At 8 h after treatment, the ATP content
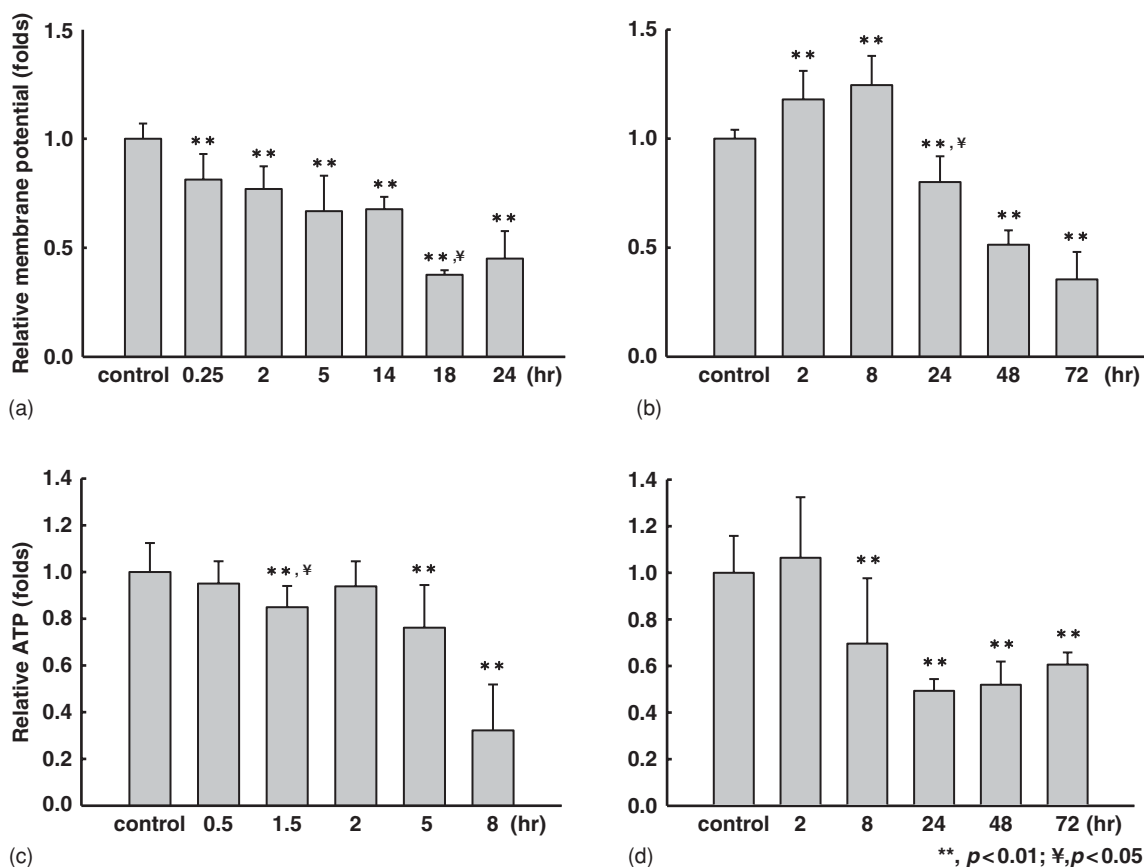
Fig. 5 The time course of the mitochondrial membrane potential ($\Delta\Psi$) [(a) and (b)] and ATP change [(c) and (d)] relative to the control before and after treatment of HeLa cells with 1 μM [(a) and (c)] and 50 nM [(b) and (d)], respectively. The control was the measurement taken before the treatment and had a value normalized to 1. Symbols ** and ¥ indicate a significant *p*-value by comparing to the control and the previous time point, respectively.

was depleted to approximately 32% (p value $= 2.32 \times 10^{-5}$) compared to controls. This is different from $\Delta\Psi$ that showed a significant increase (125 $\pm$ 13%) at the same time point. Finally, it is worth noting that the NADH fluorescence lifetime increased when both $\Delta\Psi$ and ATP were equal to or higher than their controls but long before $\Delta\Psi$ reached its maximal value [Fig. 5(b)] and ATP depletion [Fig. 5(d)]. NADH fluorescence lifetime decreased before both $\Delta\Psi$ and ATP were significantly depleted. Figure 6 summarizes the time of NADH fluorescence lifetime, $\Delta\Psi$, and ATP change in this study.

Table 1 The substrate-supported oxygen consumption rate and State 3 respiration of 50 nM STS-treated HeLa cells were measured at various time points by adding substrates of glutamate/malate and glutamate/malate plus ADP, respectively. The coupling effect between mitochondrial respiration and ATP formation was reflected by the ratio of State 3 respiration divided by the substrate-supported oxygen consumption rate.

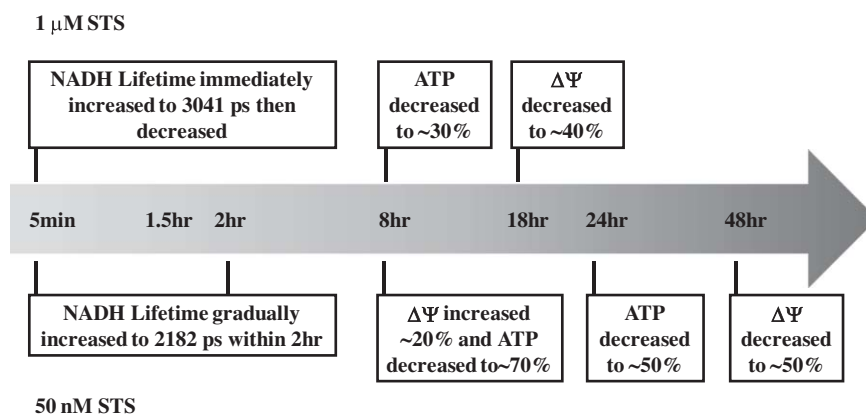|	Substrate-supported (nmole/min/10⁶ cell)	State 3 (nmole/min/10⁶ cell)	State 3 / Substrate-supported
Controls	4.06 ± 1.11	6.86 ± 2.03	1.88 ± 1.11
8 min	3.58 ± 0.90	6.79 ± 3.34	1.93 ± 0.94
30 min	2.96 ± 1.25	6.20 ± 4.52	2.03 ± 0.81
1 h	4.68 ± 2.70	6.60 ± 1.34	1.77 ± 1.11
1.5 h	4.73 ± 2.20	6.56 ± 1.90	1.46 ± 0.29
2 h	5.79 ± 2.85	6.53 ± 3.61	1.11 ± 0.07
8 h	5.80 ± 0.71	8.47 ± 2.89	1.49 ± 0.59

Fig. 6 A summary plot displays the time relationship between the NADH fluorescence lifetime, mitochondrial membrane potential ($\Delta\Psi$), and ATP content change in HeLa cells treated with 1 μM and 50 nM STS, respectively.

An elevation of $\Delta\Psi$ or mitochondrial hyperpolarization has been discovered to occur before the activation of caspases, phosphatidylserine (PS) externalization and disruption of $\Delta\Psi$ in apoptosis of cells induced by Fas-, H_2O_2-, tumor necrosis factor-, STS-, camptothecin-, and NO-, respectively.[30–33] Three main mechanisms could lead to the elevation of $\Delta\Psi$: ADP deficiency, inhibition of the enzymatic activity of F_oF_1-ATPase, and dephosphorylation of cytochrome c oxidase which is mediated by protein kinase A. STS inhibited all protein kinases including protein kinase A, which may contribute in part to the mitochondrial hyperpolarization observed in this study.

The NADH fluorescence intensity has long been used as an optical indicator of metabolism. The NADH fluorescence lifetime has recently been shown to associate with cellular metabolism as well as in manipulated human breast cells, neoplastic cells and tissues, and human mesenchymal stem cells.[14,15,24] From our measurement of the time-lapse NADH fluorescence intensity of HeLa cells treated with 50 nM STS for up to 2 h with excitation and emission wavelengths at 380 and 450 nM, respectively, using a spectrofluorometer (Hitachi F-3000, Tokyo, Japan), it showed a monochromical increase to 6-folds of the value of the control under room temperature (data not shown). Together, with the result of the lifetime measurement, we suggest that the changes of the NADH fluorescence lifetime and intensity during STS-induced apoptosis is *not* simply due to cellular metabolism change because it is neither directly associated with the oxygen consumption rate nor the intracellular ATP level. Both the oxygen consumption rate and ATP level are the indicators of the electron transport chain activity and the efficiency of the cell to generate ATP when mitochondria are highly coupled. Furthermore, because NADH fluorescence lifetime signals are directly determined by both free and protein bound NADH lifetime τ_1 and τ_2, respectively, and their relative contribution ratio (a_1-to-a_2 ratio), the results of τ_1, τ_2, and a_1-to-a_2 ratio in Fig. 3 suggested that the overall increase of mean NADH fluorescence lifetime at 50 nM dose of STS [Fig. 3(a)] was mainly attributed to both the increase in protein bound NADH fluorescence lifetime (τ_2) [Fig. 3(d)] and its contribution [i.e., decreased a_1-to-a_2 ratio in Fig. 3(b)]. These findings indicate that two conditions possibly co-existed: one is that NADH redistributed to bind to different proteins and/or binding sites; another is that the number of NADH bind-

ing sites was increased. We hypothesized that this overall increase in the intensity and lifetime of protein bound NADHs is possible because the binding partner of NADH underwent a STS-dependent conformational change (e.g., phosphorylation) or is because proapoptotic molecules reacted with mitochondria at the early phase of mitochondria-mediated apoptosis. These hypotheses still await further studies. Finally, we want to point out that the NADH fluorescence lifetime increase due to STS-induced apoptosis is significantly larger than the lifetime change due to cellular metabolism manipulation. We have monitored the NADH fluorescence lifetime change over a broad range of treatment duration under various mitochondrial inhibitors at various drug doses. The NADH fluorescence lifetime change was relatively small or unchanged.[34]

In conclusion, this study established the relationship between the NADH fluorescence lifetime change and mitochondrial dysfunction during STS-induced apoptosis. The increase and then the decrease of NADH fluorescence lifetime occurred at the early phase of apoptosis before the mitochondrial membrane potential ($\Delta\Psi$) diminished, ATP depleted, and caspase 3 activated. The lifetime increase was associated with the NADH redistribution from the free to bound form in mitochondria because both τ_1 and τ_2 were shown to increase and the a_1-to-a_2 ratio was shown to decrease. Finally, this lifetime increase due to the STS-induced cell death is significantly larger than the lifetime change caused by cellular metabolic perturbations.

References

1. S. W. Hetts, "To die or not to die: an overview of apoptosis and its role in disease," *JAMA, J. Am. Med. Assoc.* **279**(4), 300–307 (1998).
2. J. C. Reed, "Apoptosis-based therapies," *Nat. Rev. Drug Discovery* **1**(2), 111–121 (2002).

3. E. A. Schon and G. Manfredi, "Neuronal degeneration and mitochondrial dysfunction," *J Clin Invest* **111**(3), 303–312 (2003).

4. F. G. Blankenberg, "In vivo imaging of apoptosis," *Cancer Biol Ther* **7**(10), 1525–1532 (2008).

5. F. Ravandi, H. M. Kantarjian, M. Talpaz, S. O'Brien, S. Faderl, F. J. Giles, D. Thomas, J. Cortes, M. Andreeff, Z. Estrov, M. B. Rios, and M. Albitar, "Expression of apoptosis proteins in chronic myelogenous leukemia: associations and significance," *Cancer* **91**(11), 1964–1972 (2001).

6. U. Fischer, K. Janssen, and K. Schulze-Osthoff, "Cutting-edge apoptosis-based therapeutics: a panacea for cancer?" *BioDrugs* **21**(5), 273–297 (2007).

7. S. Fulda and K. M. Debatin, "Targeting apoptosis pathways in cancer therapy," *Curr Cancer Drug Targets* **4**(7), 569–576 (2004).

8. A. A. Neves and K. M. Brindle, "Assessing responses to cancer therapy using molecular imaging," *Biochim. Biophys. Acta* **1766**(2), 242–261 (2006).

9. D. Zhou, W. Chu, J. Rothfuss, C. Zeng, J. Xu, L. Jones, M. J. Welch, and R. H. Mach, "Synthesis, radiolabeling, and in vivo evaluation of an 18F-labeled isatin analog for imaging caspase-3 activation in apoptosis," *Bioorg. Med. Chem. Lett.* **16**(19), 5041–5046 (2006).

10. A. Faust, S. Wagner, M. P. Law, S. Hermann, U. Schnockel, P. Keul, O. Schober, M. Schafers, B. Levkau, and K. Kopka, "The nonpeptidyl caspase binding radioligand (S)-1-(4-(2-[18F]Fluoroethoxy)-benzyl)-5-[1-(2-methoxymethylpyrrolidinyl)s ulfonyl]isatin ([18F]CbR) as potential positron emission tomography-compatible apoptosis imaging agent," *Q. J. Nucl. Med. Mol. Imaging* **51**(1), 67–73 (2007).

11. J. A. Rosado, J. J. Lopez, E. Gomez-Arteta, P. C. Redondo, G. M. Salido, and J. A. Pariente, "Early caspase-3 activation independent of apoptosis is required for cellular function," *J. Cell. Physiol.* **209**(1), 142–152 (2006).

12. T. L. Spires-Jones, A. de Calignon, T. Matsui, C. Zehr, R. Pitstick, H. Y. Wu, J. D. Osetek, P. B. Jones, B. J. Bacskai, M. B. Feany, G. A. Carlson, K. H. Ashe, J. Lewis, and B. T. Hyman, "In vivo imaging reveals dissociation between caspase activation and acute neuronal death in tangle-bearing neurons," *J. Neurosci.* **28**(4), 862–867 (2008).

13. F. G. Blankenberg, "Imaging the molecular signatures of apoptosis and injury with radiolabeled annexin V," *Proc. Am. Thorac. Soc.* **6**(5), 469–476 (2009).

14. D. K. Bird, L. Yan, K. M. Vrotsos, K. W. Eliceiri, E. M. Vaughan, P. J. Keely, J. G. White, and N. Ramanujam, "Metabolic mapping of MCF10A human breast cells via multiphoton fluorescence lifetime imaging of the coenzyme NADH," *Cancer Res.* **65**(19), 8766–8773 (2005).

15. Y. Wu, W. Zheng, and J. Y. Qu, "Sensing cell metabolism by time-resolved autofluorescence," *Opt. Lett.* **31**(21), 3122–3124 (2006).

16. M. Tafani, D. A. Minchenko, A. Serroni, and J. L. Farber, "Induction of the mitochondrial permeability transition mediates the killing of HeLa cells by staurosporine," *Cancer Res.* **61**(6), 2459–2466 (2001).

17. H. W. Wang, V. Gukassyan, C. T. Chen, Y. H. Wei, H. W. Guo, J. S. Yu, and F. J. Kao, "Differentiation of apoptosis from necrosis by dynamic changes of reduced nicotinamide adenine dinucleotide fluorescence lifetime in live cells," *J. Biomed. Opt.* **13**(5), 054011 (2008).

18. B. Joseph, P. Marchetti, P. Formstecher, G. Kroemer, R. Lewensohn, and B. Zhivotovsky, "Mitochondrial dysfunction is an essential step for killing of non-small cell lung carcinomas resistant to conventional treatment," *Oncogene* **21**(1), 65–77 (2002).

19. A. Halestrap, "Biochemistry: a pore way to die," *Nature (London)* **434**(7033), 578–579 (2005).

20. B. Chance, B. Schoener, R. Oshino, F. Itshak, and Y. Nakase, "Oxidation-reduction ratio studies of mitochondria in freeze-trapped samples. NADH and flavoprotein fluorescence signals," *J. Biol. Chem.* **254**(11), 4764–4771 (1979).

21. C. Y. Liu, C. F. Lee, C. H. Hong, and Y. H. Wei, "Mitochondrial DNA mutation and depletion increase the susceptibility of human cells to apoptosis," *Ann. N. Y. Acad. Sci.* **1011**, 133–145 (2004).

22. Y. H. Wei, C. F. Lee, H. C. Lee, Y. S. Ma, C. W. Wang, C. Y. Lu, and C. Y. Pang, "Increases of mitochondrial mass and mitochondrial genome in association with enhanced oxidative stress in human cells harboring 4,977 BP-deleted mitochondrial DNA," *Ann. N. Y. Acad. Sci.* **928**, 97–112 (2001).

23. Y. F. Chen, C. H. Kao, Y. T. Chen, C. H. Wang, C. Y. Wu, C. Y. Tsai, F. C. Liu, C. W. Yang, Y. H. Wei, M. T. Hsu, S. F. Tsai, and T. F. Tsai, "Cisd2 deficiency drives premature aging and causes mitochondria-mediated defects in mice," *Genes Dev.* **23**(10), 1183–1194 (2009).

24. H. W. Guo, C. T. Chen, Y. H. Wei, O. K. Lee, V. Gukassyan, F. J. Kao, and H. W. Wang, "Reduced nicotinamide adenine dinucleotide fluorescence lifetime separates human mesenchymal stem cells from differentiated progenies," *J. Biomed. Opt.* **13**(5), 050505 (2008).

25. L. Michea, C. Combs, P. Andrews, N. Dmitrieva, and M. B. Burg, "Mitochondrial dysfunction is an early event in high-NaCl-induced apoptosis of mIMCD3 cells," *Am. J. Physiol. Renal. Physiol.* **282**(6), F981–F990 (2002).

26. H. D. Vishwasrao, A. A. Heikal, K. A. Kasischke, and W. W. Webb, "Conformational dependence of intracellular NADH on metabolic state revealed by associated fluorescence anisotropy," *J. Biol. Chem.* **280**(26), 25119–25126 (2005).

27. J. Yang, X. Liu, K. Bhalla, C. N. Kim, A. M. Ibrado, J. Cai, T. I. Peng, D. P. Jones, and X. Wang, "Prevention of apoptosis by Bcl-2: release of cytochrome c from mitochondria blocked," *Science* **275**(5303), 1129–1132 (1997).

28. J. Cai and D. P. Jones, "Superoxide in apoptosis. Mitochondrial generation triggered by cytochrome c loss," *J. Biol. Chem.* **273**(19), 11401–11404 (1998).

29. I. Kruman, Q. Guo, and M. P. Mattson, "Calcium and reactive oxygen species mediate staurosporine-induced mitochondrial dysfunction and apoptosis in PC12 cells," *J. Neurosci. Res.* **51**(3), 293–308 (1998).

30. A. Perl, P. Gergely, Jr., G. Nagy, A. Koncz, and K. Banki, "Mitochondrial hyperpolarization: a checkpoint of T-cell life, death and autoimmunity," *Trends Immunol.* **25**(7), 360–367 (2004).

31. J. L. Scarlett, P. W. Sheard, G. Hughes, E. C. Ledgerwood, H. H. Ku, and M. P. Murphy, "Changes in mitochondrial membrane potential during staurosporine-induced apoptosis in Jurkat cells," *FEBS Lett.* **475**(3), 267–272 (2000).

32. J. A. Sanchez-Alcazar, E. Schneider, M. A. Martinez, P. Carmona, I. Hernandez-Munoz, E. Siles, P. De La Torre, J. Ruiz-Cabello, I. Garcia, and J. A. Solis-Herruzo, "Tumor necrosis factor-alpha increases the steady-state reduction of cytochrome b of the mitochondrial respiratory chain in metabolically inhibited L929 cells," *J. Biol. Chem.* **275**(18), 13353–13361 (2000).

33. J. A. Sanchez-Alcazar, J. G. Ault, A. Khodjakov, and E. Schneider, "Increased mitochondrial cytochrome c levels and mitochondrial hyperpolarization precede camptothecin-induced apoptosis in Jurkat cells," *Cell Death Differ.* **7**(11), 1090–1100 (2000).

34. H. W. Wang, Y. H. Wei, and H. W. Guo, "Reduced nicotinamide adenine dinucleotide (NADH) fluorescence for the detection of cell death," *Anticancer Agents Med. Chem.* **9**(9), 1012–1017 (2009).